Role of amorphous and aggregate phases on field-induced exciton dissociation in a conjugated polymer

Marta M. Mróz,[1] Larry Lüer,[1] Coralie Houarner-Rassin,[2] Harry L. Anderson,[2] and Juan Cabanillas-Gonzalez[1]
[1]*Instituto Madrileño de Estudios Avanzados (IMDEA-Nanociencia), Cantoblanco, 28049 Madrid, Spain*
[2]*Chemistry Research Laboratory Department of Chemistry University of Oxford Mansfield Road, Oxford, OX1 3TA, United Kingdom*
(Received 3 October 2012; revised manuscript received 11 December 2012; published 2 January 2013)

We have applied electric field assisted pump-probe spectroscopy in order to unravel the interplay of amorphous and aggregate phases on the polaron-pair photogeneration process in a conjugated porphyrin polymer. We find that excitons photogenerated in both phases are precursors for polaron pairs with different yields. Kinetic modeling indicates a substantially larger barrier for exciton dissociation in aggregates compared to amorphous areas. The majority of polaron pairs are however formed in aggregate phases due to efficient energy transfer from the amorphous phase. Based on the change in the Stark shift associated with the photogenerated polaron density, we provide a picture of the motion of polaron pairs under the external electric field.

DOI: 10.1103/PhysRevB.87.035201 PACS number(s): 78.47.da, 78.47.jb, 78.66.Qn

I. INTRODUCTION

The primary step in the conversion of light to electricity in an organic photovoltaic device is the dissociation of an exciton under the internal field generated by the discontinuity in oxidation/reduction potentials at the donor-acceptor interface.[1–3] Bulk heterojunction solar cells (BHJSC) of conjugated polymer and the fullerene derivative PCBM contain a large density of such interfaces that act as exciton quenching centers.[4–6] In these highly inhomogeneous blends, conjugated polymers exhibit a variety of morphological phases.[7,8] Regions with enhanced interchain π overlap and exciton delocalization alternate with other areas where chains adopt a wider range of chain conformations.[9,10] Each of these regions provides a different photophysical scenario with characteristic deactivation paths competing with exciton dissociation. Accordingly, the polaron-pair photogeneration (PPG) quantum yield is not expected to be uniform in disordered conjugated polymers but to follow a strong dependence on the local polymer morphology. A complete picture of the PPG process must therefore take into account local variations in photophysics and exciton dissociation rates. Hitherto, not much attention has been placed on quantifying the contributions of polymer morphologies to the total PPG yield, probably due to the severe spectral overlap of their spectroscopic features.[11–13]

In this work, we assess the PPG process in a conjugated polymer by means of pump-probe spectroscopy under an external field. Spectral contributions to PPG from amorphous and aggregate areas of the film are singled out by probing a wide spectral range and applying global fit analysis.

We carried out this study on a *meso-meso* butadiyne-linked porphyrin polymer, (see Fig. 1). The absorption spectrum in solution of such polymers reflects a significant redshift and splitting of Q and B bands with respect to the monomer, indicating a large degree of π delocalization along the backbone as well as interaction between neighboring porphyrin macrocycles, respectively.[14,15] The solid state absorption spectrum exhibits sharpening and redshift of the Q band as well as broadening and minor shifts of transitions present in solution, indicating the coexistence of amorphous areas with aggregates on the film.[16]

Our results indicate that excitons in amorphous and aggregated regions of the polymer are precursors for charge pairs, although with very different yields. Application of an external field leads to a strong reduction in the population of both states with substantially different dissociation rates. Concomitant with exciton dissociation, a charge-induced electric field builds up due to nascent polaron pairs, which is manifested in the pump-probe spectrum as a gradual quenching of the Stark shift. The temporal evolution of the Stark signal allows us to infer the time-dependent interpair distance and associated charge mobilities during the first 50 ps after photoexcitation. We discuss the implications of these findings for understanding the performance of BHJSCs.

II. EXPERIMENTAL METHODS

A. Sample preparation and description of methods

Single-layer porphyrin polymer based diodes were fabricated in the normal way by spin coating a 3 mg/mL chloroform solution of porphyrin polymer containing 10 mg/mL of PMMA on indium tin oxide (ITO) substrates. The synthesis of the porphyrin polymer is described elsewhere.[17,18] The typical thicknesses of the spin-coated films were 70 nm. Aluminum electrodes were then thermally evaporated on the top of the film through a shadow mask to produce four pixels of the same size.

The differential reflectivity ($\Delta R/R$) was measured to resolve the generation of the primary photoexcited states in porphyrin polymeric film. Specifically, we used femtosecond pump-probe techniques with a laser system based on a Ti:Sapphire (Clark-MXR model CPA-1), delivering pulses at 1-kHz repetition rate with 780-nm center wavelength, 150-fs duration, and 500-μJ energy.[19] Here, the temporal evolution of photoexcitations is monitored by the excited-state absorption (PA) or photobleaching (PB) of photoexcited species, while the time delay is set by a computerized delay line (delay stage) between pump and probe pulses. The pump photon energy was set to 1.6 eV (780 nm) (500 Hz, 150 fs). The white light was generated in a sapphire plate (1-mm thick). Pump and probe pulses were spatially overlapped on the sample, and a computer-controlled delay stage was used to control the delay between them. The evolution of the differential reflectivity measurements was recorded over the whole visible spectrum

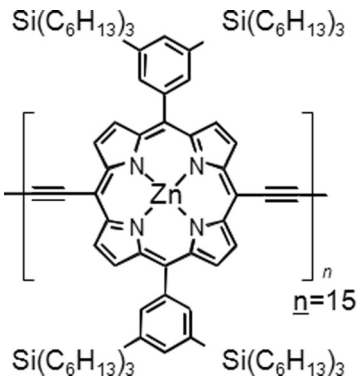

FIG. 1. Chemical structure of the porphyrin polymer.

(up to 1000 nm) using a fast optical multichannel analyzer (OMA) as a detection system.

For electric-field-assisted pump-probe spectroscopy, detection was provided by a silicon based photodiode with interferential filters (FWHM = 10 nm) for wavelength selection of the probe reflected back from the aluminum cathode surface after double transmission through the active area. A square-profile electric field modulated at 470 Hz between 0 and 1.7 MVcm^{-1} was applied across the sample, typically in reverse configuration to minimize charge carrier injection. Phase-sensitive detection was achieved by means of a lock-in amplifier referred to the frequency of the field. All the experiments were carried out at room temperature in dynamic vacuum (10^{-3} mbar).

B. Physical analysis of the pump-probe signal

In femtosecond-pump-probe spectroscopy, a pump pulse excites the sample and the relative change in transmission/reflection is measured with the probe pulse at a certain t delay. The differential reflectivity ($\Delta R/R$) is given by the change in probe intensity after double-pass of pump across the film thickness. $\Delta R/R$ is proportional to the change in the population of i states (ΔN), their effective absorption or emission cross section (σ), and the film thickness (d):[20]

$$\frac{\Delta R}{R}(\omega,t) = -\sum_{i,j}\sigma_{ij}(\omega)\Delta N(t)d. \tag{1}$$

$\Delta R/R$ thereby provides the temporal evolution of N_j photoexcited states. The electromodulated pump-probe signal (here $\Delta^2 R/R$) is given by the following expression:[21]

$$\begin{aligned}\Delta^2 R/R(\omega,t) = &-d\sum_{i,j\neq 0}\Delta_F\sigma_{i_j}(\omega,F)\Delta N_J(t)\otimes f_p\\ &-d\sum_{i}\Delta_F\sigma_{i_o}(\omega,F)N_o\\ &-d\sum_{i,j}\sigma_{i_j}(\omega)\Delta_F^2 N_J(F,t)\otimes f_p.\end{aligned} \tag{2}$$

The electric field leads to changes in cross section associated to $j\rightarrow i$ transitions ($\Delta_F\sigma_{ij}$) and in population of the excited states ($\Delta_F^2 N_j$). $\Delta_F\sigma_{ij}$ splits into two terms where the $j$state is referred to an excited ($j \neq 0$) or ground ($j = 0$) state, leading to the first two contributions, respectively, on the right-hand side of Eq. (2). Note that F and f_p stand here for the electric field and the convoluting pulse temporal profile, respectively. This latter term is taken as a step function for time domains far beyond the 150-fs temporal resolution of the experiment. Appropriate evaluation of $\Delta^2 R/R$ at different probe energies enables each of the contributions to be evaluated individually.

III. RESULTS

A. Absorption and electroreflectance spectra

Figure 2 depicts the absorption spectrum of a spin-coated porphyrin polymer film. The spectrum exhibits absorption

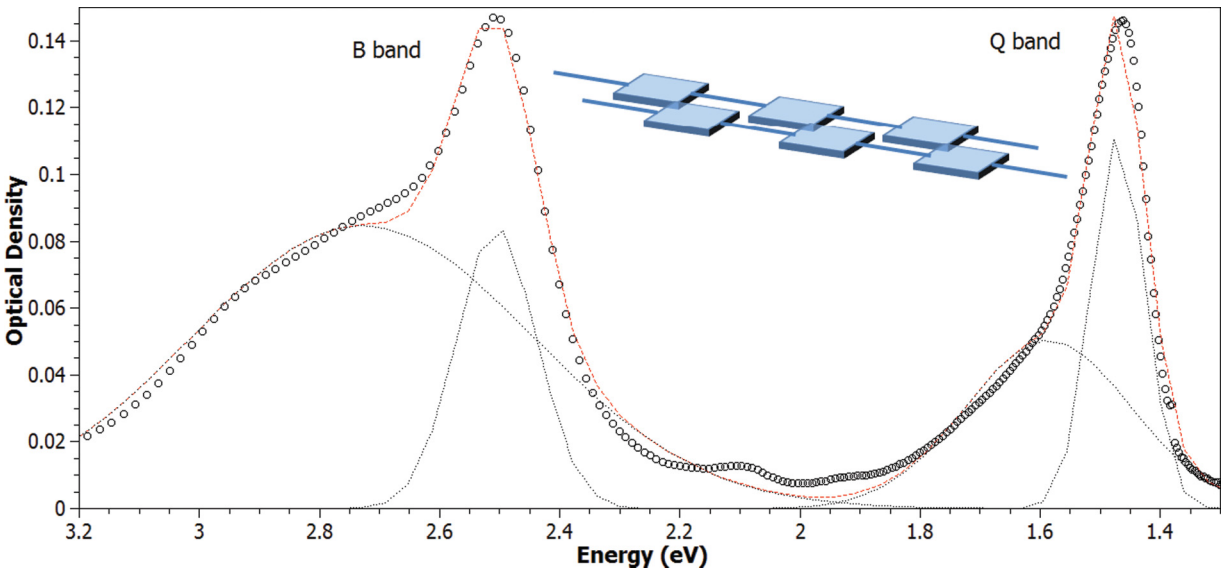

FIG. 2. (Color online) Experimental (open circle) and multipeak fitted (dashed lines) absorption spectrum of a porphyrin polymer film. The fitted absorption was obtained as a linear combination of broad and narrow Gaussian peaks assigned to amorphous areas and aggregates, respectively (dot lines). The geometrical arrangement of the aggregate is depicted in the inset.

peaks in the visible and near-IR ascribed to B and Q bands, respectively.[17] B and Q bands can be reproduced by two Gaussians with centers at 2.7, 2.5 eV (B band) and 1.6, 1.5 eV (Q band). We assign the upper and lower energy Gaussian peaks in each position to amorphous areas and aggregates respectively. The aggregate assignment is supported by low-temperature absorption and emission studies in oligomers in MTHF with chain lengths up to eight repetition units reported by Karnbratt *et al.*[22] The 150-K absorption spectra displays the presence of new narrow transitions located at 2.5 and 1.5 eV, respectively, which they attributed to π-π stacking of two planarized oligomer chains with porphyrin rings facing parallel but partially displaced, in a J-type configuration, (see inset in Fig. 2). Aggregates of butadiyne-linked conjugated porphyrin polymers typically give sharp redshifted Q bands because the backbone conformation in the aggregates tends to be more planar and π-conjugated than in the single-strand polymer.[23,24] The assignment of the upper energy Gaussian peaks to amorphous areas is justified by their spectral resemblance with the absorption spectrum in diluted solution.[14] The electroreflectance spectrum ($\Delta R/R$) of the porphyrin polymer is composed of a strong first derivative oscillation spectrally correlated to the Q band with less intense features in the visible part of the spectrum (see Fig. 3). This result is in good agreement with previous spectra reported in similar porphyrin structures with substituents at β[15] or *meso*[16] positions. Changing the polarity of the applied bias leads to the same spectral shape and almost identical $\Delta R/R$ values. This observation indicates that the field is almost entirely determined by the applied voltage with negligible contribution from injected carriers.[25] The $\Delta R/R$ spectrum at the Q-band location follows the first derivative of the Q band, having a quadratic dependence with applied voltage (inset in Fig. 3). Both observations indicate that the origin of the main electroreflectance oscillation is attributed to quadratic Stark shift of the S_1 energy level, a phenomenon which is often reported in conjugated polymer films.[26,27] The weak electroreflectance signal at the B band is related to the higher wave-function localization of S_2 respect to S_1, reflected in a lower polarizability of the former electronic state. Computational studies carried out with INDO and SCI techniques on porphyrin dimers and trimers have demonstrated in both cases that the lowest-energy transitions were comprised between orbitals delocalized over the entire π-conjugation length.[17,28]

B. Pump-probe spectroscopy

Figure 4(a) displays a 2D contour plot of transient differential reflectivity ($\Delta R/R$) as a function of wavelength and probe delay. Two positive regions are located on the blue and near-IR part of the spectrum, which correspond to a transient photobleach (hereafter named PB_1 and PB_2, respectively) separated by broad photoinduced absorption (PA). Vertical cross cuts at 0, 4, and 20-ps delay [see Fig. 4(b)] confirm that PB_1 and PB_2 are concomitant with absorption from B and Q bands, respectively, although red-shifted by about 300 meV. Interestingly, after 4 ps the low-energy tail of PB_1 and high-energy tail of PB_2 are overcome by PA, shifting the zero-crossing from 2.30 to 2.35 eV and from 1.75 to 1.60 eV, respectively. An insight into the pump-probe dynamics at 2.32 and 1.70 eV reveals that the nascent PA evolves differently in both parts of the spectrum, (see Fig. 5). The PA contribution at 2.32 eV decays in timescales exceeding

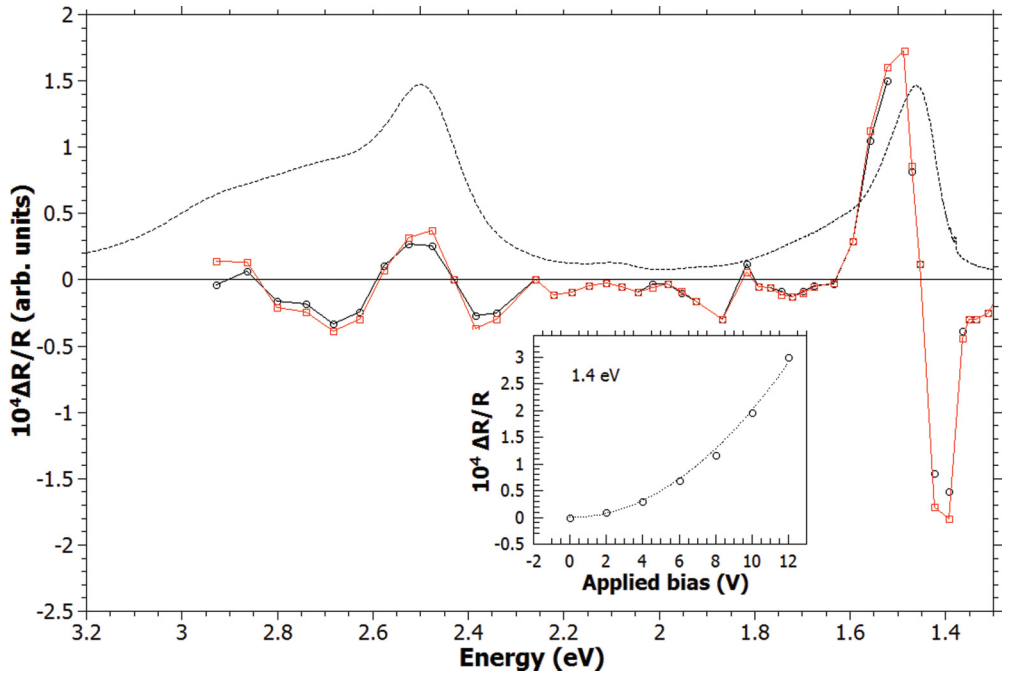

FIG. 3. (Color online) Steady-state electroreflectance spectra ($\Delta R/R$) of porphyrin polymer under an applied modulated voltage given by $V = \pm 6 \pm 6 \sin\omega t$. Open circles (squares) stand for negative (positive) applied bias. The absorption spectrum is represented by the black dash line. The dependence of the $\Delta R/R$ signal values (centered in the Q band) on the applied bias follows a quadratic law (inset).

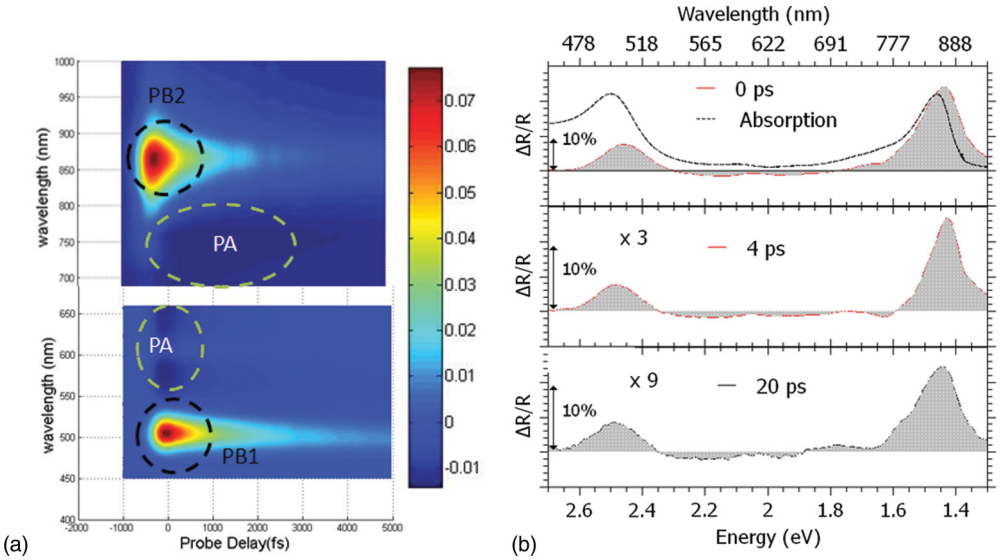

FIG. 4. (Color online) (a) Differential reflectivity ($\Delta R/R$) maps as a function of time delay and wavelength in the visible and NIR spectral region. Dashed circles are guides to the eye, highlighting photoinduced absorption (PA) and photobleach (PB) regions, respectively. (b) $\Delta R/R$ dynamics at selected time delays. The absorption spectrum is shown in the upper panel as a dashed line.

20 ps, whereas a faster decay component dominates the PA decay at 1.70 eV. Meanwhile, PB_1 (2.55 eV) and PB_2 (1.45 eV) seem to evolve following similar dynamics. We thus infer that the two overlapping PA contributions at the tails of both bands must be attributed to different excited states. Figure 6 depicts the pump-probe dynamics at 1.45 eV (PB_2) upon exciting with three different pump fluences. The acceleration of the recombination dynamics upon increasing the pump fluence clearly indicates the presence of exciton-exciton annihilation processes as one of the relaxation pathways of excited states.[29]

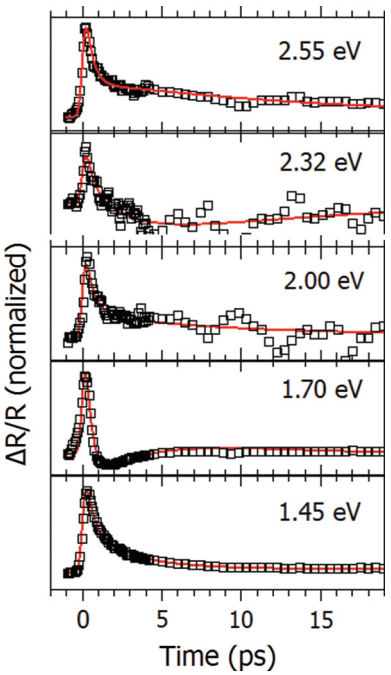

FIG. 5. (Color online) Normalized $\Delta R/R$ kinetics (open squares) of porphyrin polymer film at selected probe energies. Fits are displayed as solid lines.

C. Electric field pump-probe spectroscopy

The electric field modulated pump-probe spectra at different delays are shown in Fig. 7. The spectrum at negative delays, [see Fig. 7(a)], corresponds to the electromodulated probe reflectance unaffected by pump excitation and, as expected, it resembles the strong Stark shift feature already shown in Fig. 3. At positive delays, the pump beam photogenerates carriers, which screen the electric field on the probe area, leading to a progressive quenching of the Stark signal. Noteworthy, additional spectral features arise. The zero crossing located at negative delays at 1.46 eV shifts first to 1.48 eV at 0 ps delay and then back towards the red (1.44 eV at 60 ps delay). At 60 ps delay, the high-energy spectral region becomes broader at the expense of the low-energy spectral part. All these observations suggest that the electric field pump-probe spectrum in the porphyrin polymer is composed of a dominant transient Stark shift with contributions from other field-induced transmission changes. The electric field pump-probe dynamics are shown in Fig. 8. Dynamics at 1.48, 1.44, and 1.38 eV are vertically

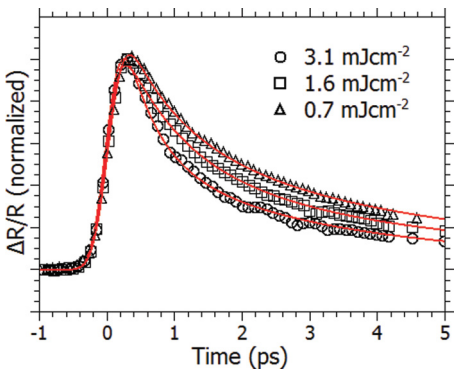

FIG. 6. (Color online) Normalized $\Delta R/R$ kinetics at 1.45 eV (PB1) under different pump fluences (open symbols). Solid lines stand for the fits obtained using the model described in the text.

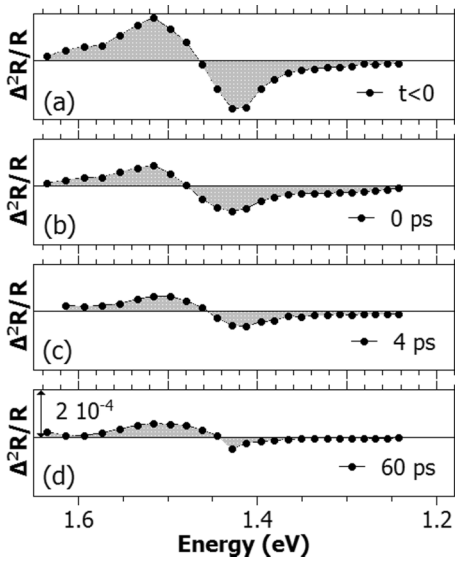

FIG. 7. Electric field assisted pump-probe spectra at different time delays: (a) $t < 0$, corresponds to electromodulated spectrum not affected by the pump presence, (b)–(d) pump-probe spectra at time delays of 0, 4, and 60 ps.

offset by a non-negligible steady-state Stark shift. At 0 ps delay, a sudden offset change occurs towards lower values, (at 1.48 and 1.46 eV), and larger values (at 1.38 eV). Interestingly, the change in offset is almost negligible at 1.44 eV, in keeping with the peak of PB_2. This oscillatory behavior points towards a field-induced shift of PB_2 as the origin of the offset change. All dynamics are characterized by a rise and decay with spectrally dependent timescales. Field-induced enhancement is observed when the probe is located within PB_2, (1.48, 1.46, and 1.44 eV), whereas field-induced quenching follows at 1.38 eV, where PB_2 is negligible and dynamics are almost exclusively ascribed to Stark shift.

IV. ANALYSIS

A. Pump probe without external field

The pump-probe data shown on Fig. 4 were reproduced with a global fit analysis involving three states (namely, X1, X2, and X3) as well as the thermally equilibrated ground state (X0). We found that the dynamics are well reproduced by a model that takes into account selective excitation of the X1 state and subsequent relaxation following a series of consecutive reactions, (X1→ X2→ X3→ X0). Details regarding the global fit analysis are found in Appendix. Fits obtained with the present model reproduced the pump-probe dynamics across the whole spectra, including the change of sign observed at 2.32 and 1.70 eV, (see Fig. 5). The resulting normalized effective cross-section spectra ($\hat{\sigma}_i$) and normalized population dynamics ($\hat{N}_i$) for X1, X2, and X3 are depicted in Fig. 9. Note that $\hat{\sigma}_i$ holds for the normalized difference between ground-state absorption cross section and the ith excited state absorption cross section. Ground-state cross sections are included in $\hat{\sigma}_i$ since every excited state leaves an

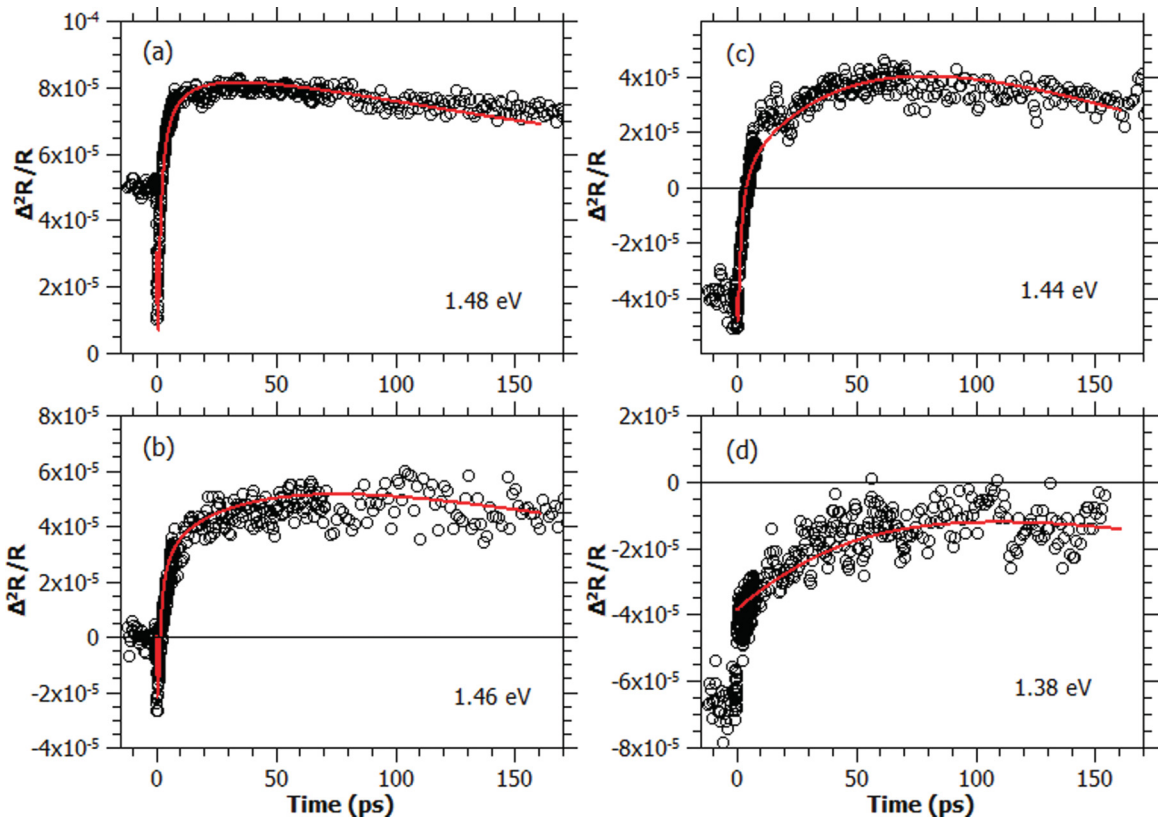

FIG. 8. (Color online) Electric field pump-probe kinetics (open circles) at (a) 1.48, (b) 1.46, (c) 1.44, and (d) 1.38 eV. Experimental data were fitted using the model describe in the text. Predicted time-dependent kinetics is displayed as solid lines.

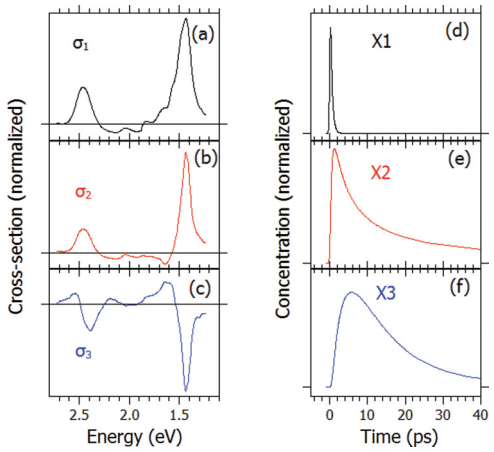

FIG. 9. (Color online) $\hat{\sigma}_i$ spectra (a)–(c) and normalized temporal population densities $\widehat{N}_i$ dynamics for X1, X2, and X3 (d)–(f) obtain from the global fit described in the text.

associated bleach of the ground-state transitions. According to our nomenclature, positive or negative $\hat{\sigma}_i$ values stand for dominant PB or PA contributions, respectively.

In the following, we discuss the spectroscopic assignment of the different excited states. The $\hat{\sigma}_1$ spectrum exhibits two positive bands located at 2.47 and 1.43 eV, being both in agreement with the lower energy part of B and Q bands (see Fig. 2). The broad negative band of $\hat{\sigma}_1$ located in the mid-visible region is instead associated with transitions from X1 to upper lying electronic levels. In order to understand the nature of X1, we first emphasize the low-excitation energy employed in this work (1.6 eV). Primary excited states are then located in the vibrational manifold of the lower singlet electronic state (S_1). It is, however, interesting that we do not observe in our pump-probe data significant spectral relaxation, so we infer that vibrational cooling of S_1 must occur on timescales below our temporal resolution of 150 fs. Typical timescales for intramolecular vibrational energy redistribution are on the 10–100 fs range.[30,31] Furthermore, the excitation energy coincides with the peak of the broad Gaussian absorption band attributed to the porphyrin amorphous phase, its large width being associated to disorder-induced inhomogeneous broadening. It thus seems plausible to ascribe X1 to a cooled S_1 excited state in the amorphous phase. The differences in bandwidth and center energies between the positive bands of $\hat{\sigma}_1$ and ground-state absorption could be explained in this framework by the narrowband pump employed that creates a spectral hole at the pumping wavelength leading to narrower bleached spectral regions. Therefore not the whole absorption band of the amorphous phase will appear as PB in the transient absorption spectrum, but only a narrow part of it. We turn now our discussion to $\hat{\sigma}_2$ and $\hat{\sigma}_3$. $\hat{\sigma}_2$ displays a negative band located at 1.60 eV as distinctive feature that overlaps with the high-energy tail of PB1. Likewise, $\hat{\sigma}_3$ exhibits negative bands at the low-energy tails of PB1 and PB2. These two observations explain well the described PA formation in the dynamics at 1.70 and 2.32 eV. This latter is likely related to the buildup of X2 and X3 states, respectively, initiated from S_1. Concerning X2, this excited state is likely to be located outside the S_1 vibronic manifold. $\hat{\sigma}_2$ has distinctive spectral features with respect to $\hat{\sigma}_1$, such as the negative band located at the high-energy tail of PB2 leading to a derivative-like feature. Contribution from triplet T_1-T_n absorption is ruled out on account of it being reported outside the PA region of interest and the long intersystem crossing in similar porphyrin polymers, which is incompatible with the observed sub-pico-second buildup.[32] Since the spectral cross section of X2 cannot be explained from the molecular electronic levels of the polymer, we believe that it must arise from electronic coupling between different polymer chromophores leading to aggregation. Owing to the Pauli principle, the one-exciton to two-exciton transitions in J aggregates are slightly lifted up in energy respect to ground to one-exciton transition. The result is a PA band almost resonant with PB but slightly blue shifted against the latter,[33,34] which explains the almost resonant positions of ground and excited state absorption in $\hat{\sigma}_2$. From the amorphous phase, resonance energy transfer (RET) is energetically possible towards the aggregated phase: the redshift of the aggregate absorption band against the amorphous phase is one necessary condition for RET to occur. The other condition is spatial proximity, requiring the domain sizes of both amorphous and aggregate regions to be in the range of the exciton diffusion lengths. This second requirement has yet to be demonstrated. From our fit estimations, the transfer time from the amorphous to the aggregate phases takes place in 500 fs. Likewise, the cross section of X3 can be understood by the superposition of PB1 and PB2 with almost resonant PA bands which are slightly redshifted in this case. A nonthermalized ground state would lead to such a PA band. Its associate PA would be redshifted respect to PB, the redshift magnitude being proportional to the amount of energy stored on the ground-state vibrational manifold. Exciton-exciton annihilation leads to the cross product of an upper lying excitonic and a ground states,[35] the energy excess being distributed among the vibrational manifold of both electronic states. From the model, we estimate that vibrational cooling of hot ground states occurs on about 7 ps in good agreement with reports in other molecular systems.[36,37]

B. Pump probe under external field

The first term in the right-hand side of Eq. (2) can be neglected since PA is almost absent in the region under study. Thus only $\Delta\sigma_{i0}$ and $\Delta^2 N_j$ contribute to $\frac{\Delta^2 R}{R}$. As displayed in Fig. 3, $\Delta\sigma_{i0}$ is manifested as a shift of $0 \rightarrow i$ transitions, which in the case of the pump-probe signal, affects both the ground state absorption and transient PB. The latter contribution appears only after pulsed excitation, leading to the sudden initial offset in electric field dynamics. The temporal evolution of $\Delta\sigma_{i0}$ provides information on the average interpair distance and charge mobility as a function of time. In parallel, the electric field also ionizes neutral states (Xn) into pairs of polarons (P^+P^-) following the expression

$$X0 + Xn \rightarrow 2X0 + P^+P^-. \tag{3}$$

According to this expression, formation of a P^+P^- pair requires two neutral states. Participation of only one ground state would imply coexistence of P^+P^- on the same chromophore. Such a scenario is likely to be present on earlier time scales that, however, are not addressed in this work.[38]

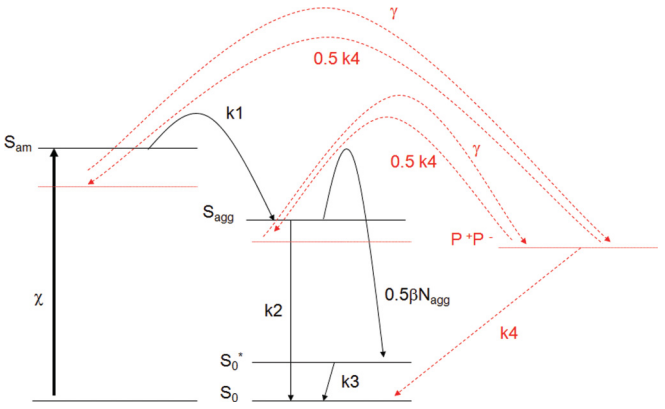

FIG. 10. (Color online) Proposed photophysical model in the presence/absence of external field. S_{am}, S_{agg}, S_0^*, and S_0 stand for excitons in amorphous and aggregate states, and hot and thermalized ground states in the aggregate, respectively. Photoexcitation is depicted by a bold arrow. Decay pathways in the absence of external field are represented by black solid arrows. Additional decay paths induced by the electric field appear as dashed red arrows. Stark shifted energy levels of S_{am} and S_{agg} are represented by red lines.

The recovery of the ground-state population is substantially modified by the field, being now governed by the P^+P^- decay kinetics. Whether the latter are significantly slower than decay kinetics of neutral states, which is often the case, the result is an increase in the intensity of the PB bands. We must remark here that we did not observe spectral features related to polaron absorption in the 1.3–3.2 eV probe region. Further details into the electric field model are found in Appendix. A scheme picture of the proposed model involving decay paths in the presence/absence of electric field is depicted in Fig. 10. Figure 11 displays the temporal evolution of the exciton dissociation rate, polaron-pair population, average polaron-pair separation, and average mobility obtained from the fits. The values of all the parameters are summarized in Table I.

V. DISCUSSION

We first focus our attention on the largely dispersive exciton dissociation rate and the role of amorphous and aggregate excitons in the overall PPG process in the polymer. At first glance, a time-dependent exciton dissociation rate is expected in our experiments, since the effective electric field in the photoexcited volume is also time dependent [see Eq. (A10) in Appendix). It is however noteworthy to compare the associated temporal kinetics of γ and F. The temporal evolution of the electric field can be obtained upon substitution of the fitting parameters displayed in Table I on Eq. (A10). The result is a gradual electric field decrease down to approximately half of the initial value after a time delay of 150 ps. Although this field screening is noticeable, it cannot account for the dramatic reduction of γ by more than three orders of magnitude observed in our results. The dependence of polaron-pair quantum yield with applied field is typically governed by Poole-Frenkel. Gulbinas *et al.* reported an enhancement in polaron-pair quantum yield below one order of magnitude upon doubling the applied bias in a

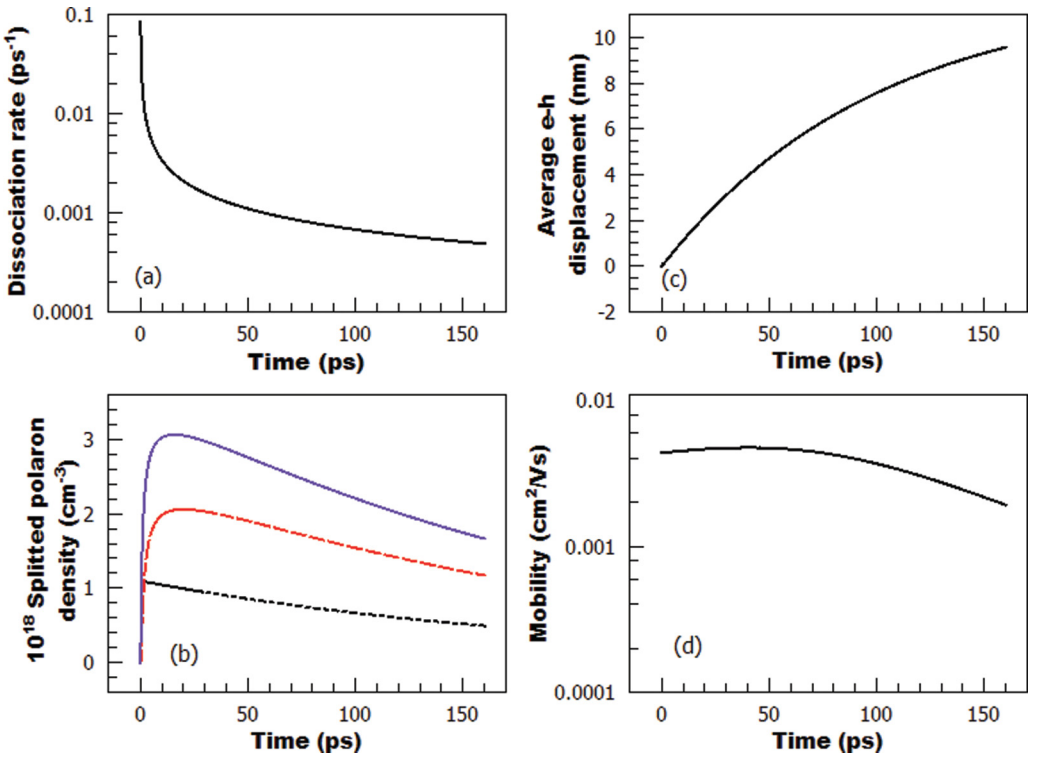

FIG. 11. (Color online) Time-dependent rates of (a) field-induced exciton dissociation, (b) polaron-pair density resulting from amorphous excitons (dotted black), aggregate excitons (dashed red) and total (solid blue), (c) average e-h separation along the field direction, and (d) average charge mobility.

TABLE I. Values of parameters employed to fit of the experimental data. k_n are recombination rates, where k_1-k_3 are monomolecular decay rates, k_4 is a polaron recombination rate, and k_5 is a rate of separation. γ is a field-induced dissociation and R_0 is a saturating e-h dist ance.

k_1 (ps^{-1})	k_2 (ps^{-1})	β(cm^3s^{-1})	k_3 (ps^{-1})	k_4 (ps^{-1})	k_5 (ps^{-1})	γ (ps^{-1})	R_0 (nm)
2.25	>0.001	7.92×10^{-9}	0.14	0.005	0.01	$0.017\, t^{-0.7}$	12

ladder-type conjugated polymer.[39] Gradual quadratic type electric field dependence was reported by Zaushitsyn *et al.* in a polythiophene derivative.[40] They observed variations within the same order of magnitude for applied fields of up to 2 $MVcm^{-1}$, i.e., the same field values as those employed in this work. We thus infer that the strongly dispersive kinetics of γ we observe must be mostly influenced by the interplay of excited states and their corresponding relaxation processes rather than electric field quenching. In fact, similar γ kinetics have been previously reported in conjugated polymers under similar fields, being interpreted in terms of cooperative effects of applied electric field and optical energy excess to the dissociation process.[41] The weaker binding energy associated with higher lying excited states is reflected in a large dissociation rate, which subsequently collapse at longer time scales as the result of exciton thermalization.[42] The decay of dissociation rate in amorphous conjugated polymers is thus the result of relaxation processes such as vibrational cooling and spectral relaxation in the density of states. Turning our discussion to the porphyrin polymer, we remark that the influence of vibrational cooling on the exciton dissociation rate is dubious. We do not observe a significant contribution from vibrational relaxation of excited states to the polymer photophysics, probably due to our limited temporal resolution. Thus the observed strong reduction in exciton dissociation rate must be attributed to spectral relaxation due to exciton diffusion from amorphous to aggregate areas. This scenario implies that the *dissociation barriers* are very different in the two areas. Pulse excitation leads to an initial population of amorphous excitons with intrinsic dissociation rates approaching 0.1 ps^{-1}. Subsequent energy transfer from the amorphous to the aggregate state is accompanied by a sudden decrease in γ indicating a significantly lower ionization probability of the latter. The polaron pair yield of each phase will be influenced by the competing deactivation pathways as well as the intrinsic exciton dissociation rates. Taking into account the decay rates involved in the photophysics as well as γ, we inferred the separate contributions to the polaron yield from amorphous and aggregated phases [see Fig. 11(b)]. The larger dissociation rate of amorphous states is for instance well counter balanced by efficient deactivation of excitons towards aggregate states in about 500 fs. On the contrary, the polaron yield from aggregates becomes predominant at long delays beyond 10 ps since γ clearly dominates over the aggregate exciton decay rate to the ground state (k_2). Despite the high ionizability of excitons in amorphous areas, the PPG process in the conjugated porphyrin appears to be mediated via population of aggregate states, which act as dissociation sites. The effect of energetic disorder on exciton dissociation was addressed by the group of Bassler and co-workers, being a good example the work by Emelianova *et al.*[43] Based on random walk theory and hopping transport in a Gaussian density of states (DOS), they calculated the dependence of charge photogeneration quantum yield as a function of temperature, electric field, and width of the DOS assuming the first hop (from exciton to a bound polaron pair) to be endothermal. Upon employing different Gaussian distributions, they observed a clear enhancement of the hopping rate with the width of the distribution. Broader distributions led also to less dramatic temperature dependencies of the hopping rate. This indicates that the energy gap between excitons and polaron-pair states is diminished by disorder, mainly due to the larger spectral overlap in the broad DOS. A side result of this is that as spectral relaxation towards the DOS tails occurs, the exciton dissociation rate slows down due to spectral overlap reduction. Field-induced PL quenching experiments performed in m-LPPP confirmed indeed this behaviour: a saturation of the quenching rate was observed to take place in the domain between 10 and 100 ps concomitant with spectral relaxation.[44,45] In the porphyrin polymer, spectral relaxation arises from efficient energy transfer from amorphous areas to aggregates with an intrinsically different DOS. Our results underlined that in certain polymers where film morphology is characterized by areas with different interchain coupling, the interplay of more than one DOS distribution must be taken into account in order to successfully describe the process of exciton dissociation. Intrinsic dissociation rates associated to the different polymer phases can differ by orders of magnitude. In the porphyrin polymer, energy transfer from loosely bound excitons in the amorphous areas to tightly bound excitons in aggregate phases becomes therefore a parasitic effect that limits PPG.

It remains to answer the question of why order facilitates charge photogeneration in BHJSCs, as suggested by several experimental evidences.[46–48] We must remark first that in a bulk heterojunction blend the charge photogeneration process is rather different from pristine polymer from the beginning since the initial step of formation of a polaron-pair state is exothermal[49] and not endothermal as in most pristine polymers. Efficient photoluminescence quenching observed in blends indicates that polaron-pair states form with very high efficiency in blends already in the absence of field.[50,51] In this latter case, the primary state is already a polaron-pair state delocalized at the donor-acceptor interface (formed either upon migration of a Frenkel exciton and encountering of a dissociating interface or by direct photoexcitation) with a lifetime typically on the order of 10 ns.[52] Thereby, assistance of energetic disorder to polaron-pair formation is no longer required in blends as in pristine polymers. In blends, the problem is then reduced to the probability for the bound electron (e) and hole (h) to escape their mutual coulombic attraction. Here factors such as energy excess of the polaron-pair state,[46] initial

mobility of e and h,[47] and high degree of charge delocalization in polymer chains with high degree of intrachain order[48] could facilitate further fission of the bound pair.

We now turn our discussion to the temporal dependence of polaron pair separation as well as mobility, [Figs. 11(c) and 11(d)]. The values obtained are averaged along the field direction so that it becomes rather hard to understand the separate contributions from charge motion inside aggregates and amorphous areas. We can however extract some conclusions based on the dimensions of the conjugated chain and the arrangement of the chains with respect to the applied field. The conformation and packing geometry of porphyrin oligomers deposited from solution by electrospray on Au substrates has been investigated with scanning tunnelling microscopy by Saywell *et al.*[53] STM images of oligomers with different chain length ranging from 4 to 40 units indicate the coexistence of regions where chains are closely packed and aligned forming lamellae with amorphous regions, characterized by chain bends and interchain crossing. In the closely packed areas, the average distance between two neighboring chains is about 2.8 nm. Whereas preferential orientation of the porphyrin core with respect to the Au(111) substrate is found in very short oligomers, such observation is not evident for long-chain polymers. Based on these findings, we infer that the maximum polaron pair separation of 9 nm in the field direction (i.e., perpendicular to the substrate) measured in our experiments must account for polarons separated among two, or at most three chains along the field direction. The fact that exciton dissociation leads to charge transfer to a neighboring chain is supported by our model, which implies the interplay of two neighbor chromophores on the dissociation kinetics Eq. (3). The random distribution of polymer chains contained in the spin-coated film is also inferred from the $0.003\ \mathrm{cm^2\ V^{-1}s^{-1}}$ initial mobility, which is substantially below the $0.084\ \mathrm{cm^2\ V^{-1}\ s^{-1}}$ mobility measured with time-resolved microwave conductivity in single porphyrin polymer chains by Grozema *et al.*[18] Although this difference is indicative of interchain motion in the film, special care is necessary when comparing mobility values. Values inferred with our experiment account for the projection along the 10^6-$\mathrm{Vcm^{-1}}$ field of the average separation between two geminate polarons. Charge motion under these conditions is likely to be influenced both by diffusion as well as field-induced drift. Values correspond then to the sum of mobilities of electrons and holes. Moreover, a maximum separation distance of 10 nm is measured at 150 ps, i.e., still below the 15–20 nm Coulomb capture radius ($\varepsilon_r \sim 3$) thus implying a non-negligible Coulombic interaction between their charges, which may also influence their relative drift. On account of these distance values, a large percentage of polaron-pairs photogenerated at donor-acceptor interfaces in BHJSCs would not survive geminate recombination. Hitherto, geminate recombination is only responsible for 20% losses in optimized devices and the reason for this low value is still under debate. At delays above 100 ps, the average distance reaches a saturation regime accompanied by a charge mobility reduction by a factor of 2. Analogous studies in PCBM films demonstrated that charge mobility kinetics are strongly field-dependent with quenching rates which cannot be accounted by electric field screening.[54] The explanation proposed for this behavior was that film morphology is characterized by discontinuity boundaries which act as shallow traps for charge motion. In our sample, such discontinuities could be represented by sites with large interchain distance to neighbor chains. Further electric field and temperature dependence studies are in prospect in order to confirm the explanation for this behavior.

VI. CONCLUSIONS

The photophysics of a disordered conjugated porphyrin polymer film is governed by two excited states associated with amorphous and aggregated areas. Upon selective excitation of amorphous areas, excitons are efficiently funneled into aggregates in timescales of 500 fs. Owing to the large aggregate population buildup, a large percentage of excitons undergo annihilation processes leading to the cross product of nonthermalized upper lying excited states as well as ground states in the aggregate. Subsequent relaxation of hot ground states occurs in about 7 ps. In the presence of an external field, both excited states dissociate with different rates implying different barriers for exciton dissociation in the two areas. The average pair interdistance is found to be below 9 nm at 150 ps implying a Coulombically bound nature of the pair and delocalization among 2–3 chains. Bound polaron pairs drift apart with an initial mobility of $310^{-3}\ \mathrm{cm^2\ V^{-1}s^{-1}}$. Excitons dissociate more easily in amorphous areas than in aggregates on account of the very different dissociation rates associated to each domain (more than two orders of magnitude larger in amorphous areas). It is often assumed that the efficiency of exciton dissociation is only related to the probability for excitons to encounter splitting interfaces during their random motion, regardless of the nature of the polymer phase at the interface. Our results indicate that this view is quite simplistic since the intrinsic dissociation rates associated to the phases may differ by orders of magnitude. In the porphyrin polymer, energy transfer of weakly bound excitons from amorphous areas to tightly bound excitons in the aggregated phases is understood as a parasitic effect which limits PPG in pristine polymers.

ACKNOWLEDGMENTS

J-CG is grateful to the Spanish Ministry of Industry and Competitivity for funding support through Ramon y Cajal program (RYC-2009-05475) and POLYDYE project (TEC2010-21830-C02-02). M. M. Mróz acknowledges support from FP7 (People) through AMAROUT program and Milan Province through DONNE AL LAVORO IN REST program.

APPENDIX

1. Equation rates in the absence of electric field

The time-dependent population of excited states is described by the following differential equations:

$$\frac{dN_0}{dt} = -\chi(t)I + k_2N_2 + k_3N_3, \tag{A1}$$

$$\frac{dN_1}{dt} = \chi(t)I - k_1N_1, \tag{A2}$$

$$\frac{dN_2}{dt} = k_1N_1 - 0.5\beta N_2^2 - k_2N_2, \tag{A3}$$

$$\frac{dN_3}{dt} = 0.5\beta N_2^2 - k_3N_3. \tag{A4}$$

Note that N_0, N_1, N_2, and N_3 hold for the population densities of X0, X1, X2, and X3, respectively, whereas $\chi(t)I$ stands for the pump induced X1 population rate, with I being the pump intensity and $\chi(t)$ a function that depends on the pulse temporal profile. For our purposes, $\chi(t)I$ was taken as an impulsive function. This equation system implies two sequential relaxation paths: X1→X2 with a monomolecular (k_1) decay rate and X2→X3 with an associated bimolecular ($0.5\beta N_2^2$) recombination term. In addition, both X2 and X3 are coupled to X0 via k_2 and k_3 monomolecular decay rates, respectively. Parameter optimization was done via an iterative process which minimized the term $\frac{\Delta R}{R}(\omega,t) - \sum_i \alpha_i \hat{\sigma}_i(\omega)\widehat{N}_i(t)$, where α_i, $\hat{\sigma}_i$, and $\widehat{N}_i$ stand, respectively, for the corresponding spectral weights, normalized *effective* cross sections (given by the superposition of all transitions associated to the i state), and normalized temporal population densities of the ith excited state. Importantly, the electric field pump-probe data were successfully reproduced by using this model embedded in a coupled differential equations system with additional field induced decay rates, as displayed in the next section.

2. Equation rates under external electric field

The field induced population changes were modeled according to the following differential equations:

$$\left.\frac{dN_0}{dt}\right|^F = -\chi(t)I + k_2\ N_2|^F + k_3\ N_3|^F - \gamma(N_1|^F + N_2|^F) + k_4 N_p, \tag{A5}$$

$$\left.\frac{dN_1}{dt}\right|^F = \chi(t)I - k_1\ N_1|^F - \gamma\ N_1|^F + 0.5k_4 N_p, \tag{A6}$$

$$\left.\frac{dN_2}{dt}\right|^F = k_1\ N_1|^F - 0.5\beta\ N_2^2\big|^F - \gamma\ N_2|^F - k_2\ N_2|^F + 0.5k_4 N_p, \tag{A7}$$

$$\left.\frac{dN_3}{dt}\right|^F = 0.5\beta\ N_2^2\big|^F - k_3\ N_3|^F, \tag{A8}$$

$$\frac{dN_p}{dt} = \gamma(N_1|^F + N_2|^F) - k_4 N_p. \tag{A9}$$

Here, $N_0|^F$, $N_1|^F$, $N_2|^F$, and $N_3|^F$ stand for the populations of X0, X1, X2, and X3 under electric field, N_p is the P^+P^- population, and γ and k_4 are, respectively, field-induced dissociation and polaron-pair recombination rates. The $\Delta\sigma_{i0}$ contribution to the dynamics is calculated by taking account of the quadratic Stark shift dependence already demonstrated, as well as the *t-dependent* effective field in the photoexcited area given by

$$F_{\text{eff}} = \frac{V_{\text{app}}}{d} - \frac{eN_pR_0[1-\exp(-k_5t)]}{\varepsilon_r\varepsilon_0}, \tag{A10}$$

V_{app} being the applied voltage, ε_r and ε_0 the relative and vacuum dielectric permittivity, respectively, e the electron charge unit, and $R_0[1-\exp(-k_5t)]$ a phenomenological term that describes the drift of electron and hole, where R_0 is the saturating distance and k_5 is the rate of charge separation.[55] The use of this expression is justified by similar time dependence reported for e-h motion in other polymer systems.[56] It also applies to disordered systems where charge transport is characterized by hopping within a density of states and thermalization leads to a progressive decrease in the hopping rate.[57]

[1] S. Guenes, H. Neugebauer, and N. S. Sariciftci, Chem. Rev. **107**, 1324 (2007).
[2] K. M. Coakley, B. S. Srinivasan, J. M. Ziebarth, C. Goh, Y. Liu, and M. D. McGehee, Chem. Matter. **16**, 4533 (2004).
[3] P. Peumans and S. R. Forrest, Chem. Phys. Lett. **398**, 27 (2004)
[4] D. Jarzab, F. Cordella, M. Lenes, F. B. Kooistra, P. W. Blom, J. C. Hummelen, and M. A. Loi, J. Phys. Chem. B **113**, 16513 (2009).
[5] M. Campoy-Quiles, T. Ferenczi, T. Agostinelli, P. G. Etchegoin, Y. Kim, T. D. Anthopoulos, P. N. Stavrinou, D. D. C. Bradley, and J. Nelson, Nat. Mater. **7**, 158 (2008).
[6] J. Peet, J. Y. Kim, N. E. Coates, W. L. Ma, D. Moses, A. J. Heeger, and G. C. Bazan, Nat. Mater. **6**, 497 (2007).
[7] Y. Gu, C. Wang, and T. P. Russell, Adv. Ener. Mater. **2**, 683 (2012).
[8] H. P. Yan, B. A. Collins, E. Gann, Ch. Wang, H. Ade, and Ch. R. McNeill, ACS Nano **6**, 677 (2012).
[9] S. T. Turner, P. Pingel, R. Steyrleuthner, E. J. W. Crossland, S. Ludwigs, and D. Neher, Adv. Funct. Mater. **21**, 4640 (2011).
[10] J. Clark, C. Silva, R. H. Friend, and F. C. Spano, Phys. Rev. Lett. **98**, 206406 (2007).
[11] M. Ariu, D. G. Lidzey, and D. D. C. Bradley, Synth. Met. **111-112**, 607 (2000).
[12] M. Yan, L. J. Rothberg, E. W. Kwock, and T. M. Miller, Phys. Rev. Lett. **75**, 1992 (1995).
[13] T. Virgili, D. Marinotto, C. Manzoni, G. Cerullo, and G. Lanzani, Phys. Rev. Lett. **94**, 117402 (2005).
[14] M. U. Winters, J. Karnbratt, M. Eng, C. J. Wilson, H. L. Anderson, and B. Albinsson, J. Phys. Chem. C **111**, 7192 (2007).
[15] H. L. Anderson, S. J. Martin, and D. D. C. Bradley, Angew. Chem., Int. Ed. Engl. **33**, 655 (1994).
[16] T. E. O. Screen, K. B. Lawton, G. S. Wilson, N. Dolney, R. Ispasoiu, T. Goodson III, S. J. Martin, D. D. Bradley, and H. L. Anderson, J. Mater. Chem. **11**, 312 (2001).
[17] H. L. Anderson, Chem. Commun. **23**, 2323 (1999).
[18] F. C. Grozema, C. Houarner-Rassin, P. Prins, L. D. A. Siebbeles, and H. L. Anderson, J. Am. Chem. Soc. **129**, 13370 (2007).
[19] D. Polli, L. Luer, and G. Cerullo, Rev. Sci. Instrum. **78**, 103108 (2007).
[20] T. Virgili, J. Cabanillas-Gonzalez, L. Luer, and G. Lanzani, in *Photophysics of Molecular Materials*, edited by G. Lanzani (Wiley-VCH, Weinheim, Germany, 2006).
[21] J. Cabanillas-Gonzalez, G. Grancini, and G. Lanzani, Adv. Mater. **23**, 5468 (2011).
[22] J. Kärnbratt, M. Gilbert, J. K. Sprafke, H. L. Anderson, and B. Albinsson, J. Phys. Chem. C **116**, 19630 (2012).
[23] H. L. Anderson, Inorg. Chem. **33**, 972 (1994).

[24]T. E. O. Screen, J. R. G. Thorne, R. G. Denning, D. G. Bucknall, and H. L. Anderson, J. Mater. Chem. **13**, 2796 (2003).
[25]J. M. Lupton, C. Im, and H. Bassler, J. Phys. D: Appl. Phys. **36**, 1171 (2003).
[26]M. G. Harrison, S. Möller, G. Weiser, G. Urbasch, R. F. Mahrt, H. Bässler, and U. Scherf, Phys. Rev. B **60**, 8650 (1999).
[27]P. J. Brown, H. Sirringhaus, M. Harrison, M. Shkunov, and R. H. Friend, Phys. Rev. B **63**, 125204 (2001).
[28]D. Beljonne, G. E. O'Keefe, P. J. Hamer, R. H. Friend, H. L. Anderson, and J. L. Brédas, J. Chem. Phys. **106**, 9439 (1997)
[29]J. Cabanillas-Gonzalez, C. Sciascia, G. Lanzani, S. Toffanin, R. Capelli, M. C. Ramon, M. Muccini, J. Gierschner, T. Y. Hwu, and K. T. Wong, J. Phys. Chem. B **112**, 11605 (2008).
[30]T. Elsaesser and W. Kaiser, Annu. Rev. Phys. Chem. **42**, 83 (1991).
[31]H. Kano and T. Kobayashi, J. Chem. Phys. **116**, 184 (2002).
[32]M. K. Kuimova, M. Hoffmann, M. U. Winters, M. Eng, M. Balaz, I. P. Clark, H. A. Collins, S. M. Tavender, C. J. Wilson, B. Albinsson, H. L. Anderson, A. W. Parker, and D. Phillips, Photochem. Photobiol. Sci. **6**, 675 (2007).
[33]M. van Burgel, D. A. Wiersma, and K. Duppen, J. Chem. Phys. **102**, 20 (1995).
[34]J. Knoester, Phys. Rev. A **47**, 2083 (1993).
[35]T. Q. Nguyen, I. B. Martini, J. Liu, and B. J. Schwartz, J. Phys. Chem. B **104**, 237 (2000).
[36]I. Delfino, C. Manzoni, K. Sato, C. Dennison, G. Cerullo, and S. Cannistrato, J. Phys. Chem. B **110**, 17252 (2006).
[37]S. Shim and R. A. Mathies, J. Phys. Chem. B **112**, 4826 (2008).
[38]A. Devizis, K. Meerholz, D. Hertel, and V. Gulbinas, Chem. Phys. Lett. **498**, 302 (2010).
[39]V. Gulbinas, Y. Zaushitsyn, V. Sundström, D. Hertel, H. Bässler, and A. Yartsev, Phys. Rev. Lett. **89**, 107401 (2002).
[40]Y. Zaushitsyn, V. Gulbinas, D. Zigmantas, F. Zhang, O. Inganäs, V. Sundström, and A. Yartsev, Phys. Rev. B **70**, 075202 (2004).
[41]W. Graupner, G. Cerullo, G. Lanzani, M. Nisoli, E. J. W. List, G. Leising, and S. De Silvestri, Phys. Rev. Lett. **81**, 3259 (1998).
[42]T. Virgili, J. Clark, J. Cabanillas-Gonzalez, L. Bazzana, K. C. Vishnubhatla, R. Osellame, R. Ramponi, and G. Lanzani, J. Mater. Chem. **20**, 519 (2010).
[43]E. V. Emelianova, M. Van der Aweraer, and H. Bässler, J. Chem. Phys. **128**, 224709 (2008).
[44]R. Kersting, U. Lemmer, M. Deussen, H. J. Bakker, R. F. Mahrt, H. Kurz, V. I. Arkhipov, H. Bässler, and E. O. Gobel, Phys. Rev. Lett. **73**, 1440 (1994).
[45]M. Scheidler, U. Lemmer, R. Kersting, S. Karg, W. Riess, B. Cleve, R. F. Mahrt, H. Kurz, H. Bässler, E. O. Gobel, and P. Thomas, Phys. Rev. B **54**, 5536 (1996).
[46]A. A. Bakulin, A. Rao, V. G. Pavelyev, P. H. M. van Loosdrecht, M. S. Pshenichnikov, D. Niedzialek, J. Cornil, D. Beljonne, and R. H. Friend, Science **335**, 1340 (2012).
[47]C. Deibel, T. Strobel, and V. Dyakonov, Phys. Rev. Lett. **103**, 036402 (2009).
[48]C. Schwarz, H. Bässler, I. Bauer, J.-M. Koenen, E. Preis, U. Scherf, and A. Köhler, Adv. Mater. **24**, 922 (2012).
[49]T. Agostinelli, M. Caironi, D. Natali, M. Sampietro, G. Dassa, E. V. Canesi, C. Bertarelli, G. Zerbi, J. Cabanillas-Gonzalez, S. De Silvestri, and G. Lanzani, J. App. Phys. **104**, 114508 (2008).
[50]J. Cabanillas-Gonzalez, T. Virgili, G. Lanzani, S. Yeates, M. Ariu, J. Nelson, and D. D. C. Bradley, Phys. Rev. B **71**, 014211 (2005).
[51]J. Cabanillas-Gonzalez, J. Nelson, D. D. C. Bradley, M. Ariu, D. G. Lidzey, and S. Yeates, Synth. Met. **137**, 1471 (2003).
[52]D. Veldman, O. Ipek, S. C. J. Meskers, J. Sweelssen, M. M. Koetse, S. C. Veenstra, J. M. Kroon, S. S. van Bavel, J. Loos, and R. A. J. Janssen, J. Am. Chem. Soc. **130**, 7721 (2008).
[53]A. Saywell, J. K. Sprafke, L. J. Esdaile, A. J. Britton, A. Rienzo, H. L. Anderson, J. N. O'Shea, and P. H. Beton, Angew. Chem., Int. Ed. Engl. **49**, 9136 (2010).
[54]J. Cabanillas-Gonzalez, T. Virgili, A. Gambetta, G. Lanzani, T. D. Anthopoulos, and D. M. De Leeuw, Phys. Rev. Lett. **96**, 106601 (2006).
[55]J. Cabanillas-Gonzalez, T. Virgili, L. Luer, G. Lanzani, T. D. Anthopoulos, and D. M. De Leeuw, Phys. Rev. B **75**, 045207 (2007).
[56]I. G. Scheblykin, A. Yartsev, T. Pullerits, V. Gulbinas, and V. Sundstrom, J. Phys. Chem. B **111**, 6303 (2007).
[57]B. Hartenstein, H. Bassler, A. Jakobs, and K. W. Kehr, Phys. Rev. B **54**, 8574 (1996).